Structure of photoexcitation cross sections of electric dipole resonance in spherical nuclei

S. N. Belyaev, O. V. Vasil'ev, A. A. Nechkin, and V. A. Semenov
Institute of Mathematical Physics, Saratov State University

V. V. Voronov and V. Yu. Ponomarev
Joint Institute for Nuclear Research, Dubna

Fiz. Elem. Chastits At. Yadra **23**, 1537–1571 (November–December 1992)

Photoneutron cross sections have been measured in some spherical nuclei by the bremsstrahlung technique. The aim was to find intermediate structure in the interval of energies from the reaction threshold up to 25 MeV. Structure has been found in the low-energy cross sections of nuclei near lead. The experimental data are compared with the results of calculations in the quasiparticle–phonon nuclear model.

1. INTRODUCTION

Properties of high-lying collective nuclear states such as giant multipole resonances are still being actively investigated by many research groups. The rapid progress of experimental techniques has significantly extended the range of beams that can be used and has made possible coincidence experiments, which give new information about the intrinsic structure of the resonances. Many results of these investigations, both experimental and theoretical, have been systemized in the reviews of Refs. 1–9. Study of giant multipole resonances continues actively.

The electric giant dipole resonance has been studied better than other excitations. The reasons for this are both historical—it was the first to be discovered, and data on it exist for most nuclei—and due to the fact that it can be studied by the photoexcitation reaction, which is relatively easy to realize. Indeed, a significant fraction of the data on the E1 resonance have been obtained in photon reactions.

For $A \geqslant 100$ nuclei, the high Coulomb barrier means that the photoabsorption cross section is effectively exhausted by the photoneutron channels. The contribution from excitations of nondipole type is only a few percent of the integrated reaction cross section in the range of energies from the neutron emission threshold to 25 MeV. Therefore, the structure of the cross section obtained in the (γ,n) reaction must reflect the real distribution of the dipole strength. This selectivity of the reaction makes it possible to test the results of calculations of E1 excitations in models by comparison with the experimental data.

The main results on photoneutron cross sections have been obtained in measurements using bremsstrahlung and quasimonochromatic gamma-ray beams. For the latter experimental method, the data and their interpretation are covered quite fully in the reviews of Refs. 1 and 10, and the parameters of the Lorentz lines that approximate the cross sections and estimates of the integrated cross sections are given in Ref. 11.

The description of the shape of the cross sections by means of lines of Lorentz type is based on the classical notion of the vibrations of a dipole in the field of an electromagnetic wave.[12] The values of the parameters are used in comparisons with theoretical estimates and also as empirical estimates needed in the models themselves if such estimates cannot be obtained in them (this applies mainly to the damping width). In such an approach, intermediate structure in the cross section cannot be explained, and therefore systematic study of the shape of the cross sections for medium and heavy nuclei was not made for a long time. There were also experimental difficulties with investigating these relatively small effects, which often merely distort the line shape.

Data on intermediate structure are available only for individual nuclei, mainly with $A \sim 200$. It appears that Fuller and Hayward[13] were the first to consider the features in the (γ,n)-reaction cross sections on $^{206-208}$Pb and ^{209}Bi, pointing out the possibility of describing the cross sections by a simple Lorentz line, the "shoulder" in the ^{208}Pb cross section near 12 MeV, and the presence of structure in the threshold region. The existence of a peak in the cross section of the reaction on ^{208}Pb at ~ 11.5 MeV was noted in Ref. 14. The results of study of intermediate structure in several nuclei (including ^{208}Pb and ^{90}Zr) are given in Ref. 10. Possibly because of an incorrect method of calculating the cross sections from the photoneutron yields, these data cannot be readily interpreted and disagree with the more recent measurements of Refs. 15 and 16, which were made by different methods and agree well with each other. Cross sections of (γ,n) reactions on ^{141}Pr were obtained in several studies,[17–21] but they exhibit appreciable discrepancies in the shapes of the curves, moreover not only in the low-energy part. It is obvious that when such data are analyzed the very existence of structure in cross sections of the reactions on medium and heavy nuclei can be doubted (see, for example, Ref. 22).

At the same time, the information (both qualitative and quantitative) on the positions of the structures in the cross sections and on their contributions to the integrated cross section does match the results obtained in theoretical calculations in a number of models.[23–25] The explanation of the observed structures and the damping mechanism for the giant dipole resonance is also important. Numerous theoretical studies (Refs. 3–9 and 23–28) have established that the main mechanism responsible for the damping of the giant multipole resonance is coupling of simple

 0090-4759/92/060667-17$04.00

particle–hole states to more complicated two-particle–two-hole states, the coupling to the low-lying vibrational modes being the most important.

In this review, we consider the results obtained in recent years from the study of the shape of the photoneutron cross sections in measurements using a bremsstrahlung γ beam and an analysis of the experimental data on the basis of the quasiparticle–phonon nuclear model (Refs. 4, 8, 29, and 30).

2. EXPERIMENTAL METHOD

The bremsstrahlung method was used in the experimental study of the structure of the (γ,n)-reaction cross sections. In it one measures the yields of photoneutrons from a sample irradiated with electron bremsstrahlung γ rays. The cross sections are calculated from the measured data. The electron accelerator used for the measurements was a betatron with maximum energy 25 MeV. The multichannel method[31] with the experiment controlled by an on-line computer was used. The maximum energies $E_{\gamma\,\max}$ of the bremsstrahlung beam in each channel, the order of scanning in the energy, and the statistical accuracy of the measurements were determined by the resolution in the cross sections that was desired.

In the method, the (γ,n)-reaction cross section is obtained by solving a Fredholm integral equation of the first kind—the inverse problem for recovering a function from the experimental data. The employed method of calculation must fully exploit the experimental data and give reliable information on the cross-section structure. Obviously, the quality of the result can be affected both by the errors of the measurement and by instrumental errors and errors in the method of analyzing the data. It is therefore necessary to estimate the physical significance of the structures in the cross section by making test measurements on nuclei having a complicated shape of the cross section (as for ^{16}O) and on a numerical experiment.

The (γ,n)-reaction cross section in an experiment is always some approximation of the real line, of which all one can say with certainty is that it is continuous (though even here exceptions are possible for light nuclei). The shape of the cross sections is deduced from the available experimental data and theoretical ideas about the mechanism of nuclear photoexcitation. This means that when an experiment is planned one does not know in advance the level of resolution that will be sufficient to reproduce all the structures in the line of the cross section. Since the resolution and confidence level with which the structures are obtained are directly related to the degree of discretization of the measured yield curve, it is desirable to perform the experiments with the least possible step in $E_{\gamma\,\max}$ and with the statistical accuracy necessary for such a step. From this point of view, the bremsstrahlung and quasimonochromatic methods encounter some difficulties in the study of photoexcitation in the region of giant dipole resonances. For the first, a decrease of the step in the measurements makes it necessary to increase the measurement time and the number of points with respect to $E_{\gamma\,\max}$. This requires high stability in the operation of the apparatus and correct analysis of the data, since the condition of the system of equations deteriorates. For the second method, the fact that the beam is not perfectly monochromatic makes it impossible to resolve structures with widths $\approx$100 keV, and a spread of points in the cross section determined by the statistics is observed. The use of these cross sections as photoneutron yields brings us back to the problems of the bremsstrahlung method with the addition of the fact that the γ-ray spectrum does not have an analytic form.

Thus, the experimental data obtained in the considered work were made possible by fulfillment of two conditions: 1) the photoneutron yields were measured with a small step and the required accuracy;[32] 2) the cross sections were calculated by the method of statistical regularization of Refs. 33–40, based on use of the probabilistic character of the experimental values.

3. MEASUREMENT TECHNIQUE

Quantities directly measured in the experiment are the photoneutron yield $N(E_{\gamma\,\max})$ and the γ-radiation dose $D(E_{\gamma\,\max})$, which is measured by a scintillation pulse dosimeter.[41] These measurements are made for each γ pulse for a given number of $E_{\gamma\,\max}$ values. In the intervals between the pulses, the random variable $N(E_{\gamma\,\max})/D(E_{\gamma\,\max})$ and the statistics sufficient for it are calculated, making it possible to determine at any stage of the experiment the sample mean and variance. The photoneutron yield per unit dose $Y(E_{\gamma\,\max})$ is obtained by normalizing the values to the readings of an aluminum absolute chamber having design sensitivity from $E_{\gamma\,\max}$.[42]

The regime of scanning with respect to $E_{\gamma\,\max}$ is done by means of the betatron energy control system, which contains the following main blocks (see Fig. 1): 1) an electronic integrator, which converts the voltage from a slave coil on the betatron pole into a voltage that replicates the shape of the magnetic field on the equilibrium orbit; 2) a digital-to-analog converter (DAC) that gives a constant voltage proportional to the required energy of the accelerated electrons in response to a digital code loaded by the computer; 3) a comparator that develops a pulse when the magnetic-field analog voltage is equal to the voltage from the DAC; 4) a circuit for producing a powerful current pulse to deflect the accelerated electrons onto the bremsstrahlung target.

The 10-digit DAC makes it possible to generate arbitrary sequences of betatron energies at discrete intervals of 20 keV, covering the entire region of the giant dipole resonance. The maximum instability of the scale does not exceed 20 keV at high energies. The absolute calibration of the betatron energy scale was established from the thresholds of the (γ,n) reactions on ^{207}Pb, ^{209}Bi, ^{63}Cu reactions and the break in the ^{16}O(γ,n) yield curve at E=25 MeV.

The photoneutron detector consisted of 90 BF_3 counters in paraffin, uniformly distributed parallel to the through channel in which the sample was placed. The counters were combined into 15 groups with six in each, forming 15 independent detection channels consisting of an amplifier, an integral discriminator, and a 4-bit double counter, to which there is program access. The detector

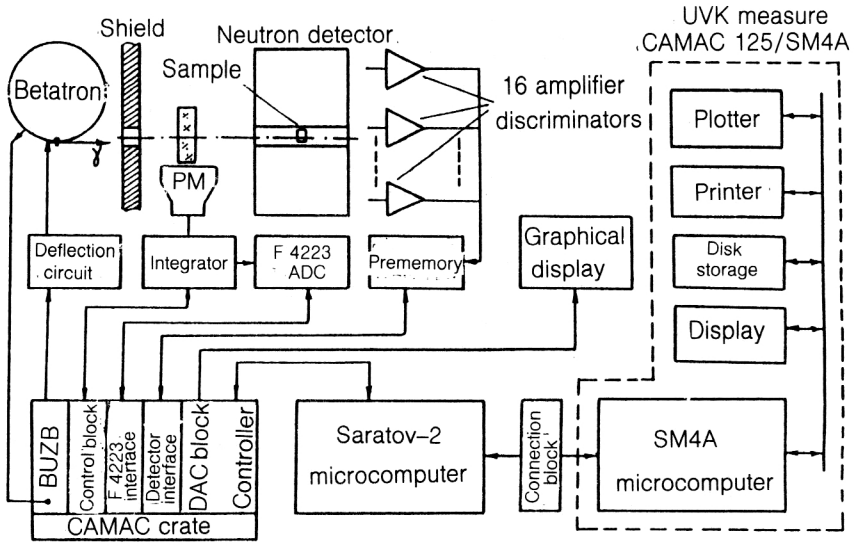

FIG. 1. Schematic diagram of automated measurement of photoneutron yields with an on-line computer by the multichannel method and using a bremsstrahlung beam.

efficiency was 20%, and the lifetime of thermal neutrons in it was 126 μsec. A feature of the neutron-detection channel is that the position and duration of the "gates" during which the neutrons are counted are controlled by the program. During the scanning with respect to the betatron energy, this makes it possible to change the neutron-detection efficiency in order to reduce the counting rates to acceptable values, particularly in the case of thick targets. This device significantly improves the efficiency with which the operating time of the accelerator is exploited.

A nontraditional element in the bremsstrahlung experiments is the scintillation pulse dosimeter of the γ rays incident on the target. The scintillator is plastic of thickness 2 mm, thick that is intersected by the beam. The current pulse from a photomultiplier is integrated, the result is stored, and then, by means of an ADC of type F4223 (coding time 3 μsec, 11-bit accuracy), is transformed into a digital code and read by the computer, in which it is used to normalize the measured neutron yield in the given accelerator cycle.

In the experiment, much attention was devoted to visualization of the incoming information. The neutron yields from the channels, the calculated statistics, and the pulse dose were shown on graphical displays. The operative control of the pulse dose is particularly important, since it reflects the quality of operation of the betatron.

The measuring complex includes a Saratov-2 microcomputer (of type PDP-8), which collects and stores the information, makes the necessary calculations, and controls the betatron. All elements of the facility requiring program control are executed in the form of CAMAC blocks or have interfaces in a crate. The Saratov-2 computer is connected to a higher-level computer of type SM4A, which has a developed periphery: display, disk memory of about 50 Mbyte, printers, and graphical plotter. It is at this level that the stored information is kept, the problem of obtaining the spectrum is solved, and the control programs for the Saratov-2 computer are prepared and modified. The control from the operating panel during the measurements is also done at this level. Thus, the entire process of obtaining and analyzing the data during the experiment is fully automated and does not require "manual" corrections. This increases the reliability of the results.

4. MEASUREMENT OF THE EXPERIMENTAL CROSS SECTIONS OF THE (γ,n) REACTIONS

The experimental results obtained by using the bremsstrahlung method are the mean photoneutron yield and its variance at given points with respect to $E_{\gamma\,\max}$. After corrections have been introduced for the background and losses, and the yield has been reduced to unit dose, the data are used to calculate the (γ,n) cross section. This involves solving an integral equation of the form

$$\int_{B_n}^{E^i_{\gamma\,\max}} \Phi(E^i_{\gamma\,\max}, E^i_\gamma)\sigma_{\exp}(E_\gamma)dE_\gamma = Y(E^i_{\gamma\,\max}), \qquad (1)$$

where $\Phi(E^i_{\gamma\,\max})$ is the shape of the bremsstrahlung spectrum, $Y(E^i_{\gamma\,\max})$ is the reduced photoneutron yield, and $\sigma(E_\gamma)$ is the experimental cross section, which, because of the small contribution of the other partial cross sections, is effectively equal to the sum $\sigma(\gamma,n)+\sigma(\gamma,2n)$.

Equation (1) represents an inverse problem, the difficulties of solving which are due to the fact that its right-hand side contains not exact values but estimates from a limited sample—a realization of a random process. Therefore, the problem is improperly posed, and one can obtain for it only an approximate solution selected on the basis of certain criteria from a set of other data that also satisfy Eq. (1).

In the review of Ref. 33 there is a detailed discussion of inverse problems associated with recovery of unknown functions from experimental data together with an exposition of an approach to their solution developed in Refs. 34–37 using the probabilistic nature of the results of the measurements. We used the statistical regularization method developed on this basis to recover the cross sections. In the method, the solution of Eq. (1) is sought in an ensemble of smooth functions belonging to a certain distribution. The density of this distribution is the *a posteriori*

probability density for the existence of a solution σ for a given value of Y determined by the Bayes formula:

$$P(\sigma/Y)=P(\sigma)P(Y/\sigma), \quad (2)$$

where $P(\sigma)$ is the *a priori* probability density, the form of which is determined by the requirement of minimum information on σ and the condition of smoothness of σ (in our calculations, the minimum of the norm of the second derivative is used); $P(Y/\sigma)$ is the conditional density of the probability for obtaining the given value of Y under the condition that σ exist. This distribution characterizes the experiment. In our case, the values of the measured yield $Y(E_{\gamma\,\max})$ are sample means of random variables and, therefore, are also normally distributed random variables. The deviation of these values from the ideal values (for given σ) can be specified by some distribution law of the deviations. It is assumed that this distribution is Gaussian with variance equal to the experimental variance $(\Delta Y)^2$ of the photoneutron yield.

Our computational scheme also uses the condition of non-negativity of the unknown function, and an *a posteriori* estimate of the errors of the original data is calculated.[38] The solution σ—a function of the most probable smoothness—is found by the method of the maximum of the *a posteriori* probability density, and the error $\Delta\sigma$ is determined as the square root of the variance of this distribution.

The basic formulas, the ideas of the algorithms and their program realization, and the results of application of the method to some specific problems are given in Refs. 39 and 40. For our calculation of the cross sections, the changes only concerned the problems of algebrization of Eq. (1) with kernel in the form of an analytic expression for the shape of the bremsstrahlung spectrum[42] and the use of a different algorithm to find the parameters α and β (the parameters of the smoothness and of the estimate of the errors in the initial data). The latter arises because of the need to shorten significantly the computing time in calculations with a large number of points and to be sure of finding solutions for all initial data.

The use of this method makes it possible to analyze data measured with an arbitrary step in $E_{\gamma\,\max}$. The weight of each yield point is taken into account, and nothing that is not present in the experimental data is introduced into the recovered function. It is not necessary to make a preliminary processing (smoothing, etc.) of the initial data, or to intervene in the process of calculation or carry out any actions to correct the result. It should be noted that the initial data contain more complete information about the cross section than the recovered function. The reason for this is the averaging of the structures (if they are present, a fact that, in general, is not known in advance) in the cross section on account of the finite number of points used to discretize the energy scale in cases when the measurement step is comparable with the width of the structures. Therefore, when planning an experiment to study cross-section structure, one must bear in mind that the conditions of the measurements themselves determine the final result. Since we do not know the actual cross section and the degree of its complexity, the choice of the conditions and the influence of the solving procedure can be estimated either empirically (by changing a parameter of the experiment) or by performing a numerical experiment. We shall consider these estimates later when discussing the resolution in the experiment.

The photoneutron cross section of the (γ,n) reaction is obtained from the calculated $\sigma_{\exp}(E_\gamma)$ after the introduction of a correction for the multiplicity beyond the threshold of the $(\gamma,2n)$ reaction. For this we use the expression obtained on the basis of the statistical theory:[43]

$$\sigma(\gamma,Tn)=\sigma_{\exp}(E_\gamma)/(2-f), \quad (3)$$

where $f=(1+x)\exp(-x)$ for $x=(E_\gamma-B_{2n})a^{1/2}\times(E_\gamma-B_n)^{-1/2}$. Here, B_n and B_{2n} are the thresholds of the reactions with emission of one and two neutrons, and a is a level-density parameter determined by fitting (3) to the data on $\sigma(\gamma,n)$ and $\sigma(\gamma,2n)$ measured by means of the quasimonochromatic method.[11]

Since we did not make absolute measurements, the cross sections were reduced to absolute values, using as a monitor the data from Ref. 11. For example, for the nuclei with $N=82$ and ^{208}Pb the normalization was based on comparison of the data on ^{142}Nd with the values calculated from the parameters of the Lorentz line given in Ref. 11 for the cross section of the reaction on ^{142}Nd measured at Saclay. The fit was made using integrated cross sections in the interval of energies in the region of the cross section maximum before the threshold of the $(\gamma,2n)$ reaction.

5. ESTIMATE OF THE ENERGY RESOLUTION

It can be regarded as undisputed that the cross sections of (γ,n) reactions are curves of resonance form of different degrees of smoothness. However, the shape of the curves is unknown, and therefore we cannot compare them with experimental curves and estimate the resolution level by comparing the parameters (for example, amplitudes and widths) of structures, if such exist.

In direct measurements, the resolution will be determined by the monochromaticity of the γ-ray beam. Factors such as the measurement steps, the accuracy with which the energy is specified, and the statistics will affect only the volume and quality of the information on the cross section.

In our bremsstrahlung method, the real information about the cross section is contained in the values of the photoneutron yield and its variance. Here, the measurement step, the accuracy, and the stability of operation of the apparatus are important, since structures having an "experimental" origin or smoothing of real structures can occur in the recovered cross section. As a good illustration of this, we can consider the shape of the reaction cross section on ^{208}Pb in the threshold region. Measurements with different steps (50, 25, 40 keV in Fig. 2; 10 keV in Fig. 3) and with different statistics (in deteriorating order) show both a change in the amplitudes and widths of the peaks at 7.6 and 8 MeV and the appearance (and disappearance) of a structure at energy $\approx$7.43 MeV. A dependence on only the measurement step can be seen in Fig. 3,

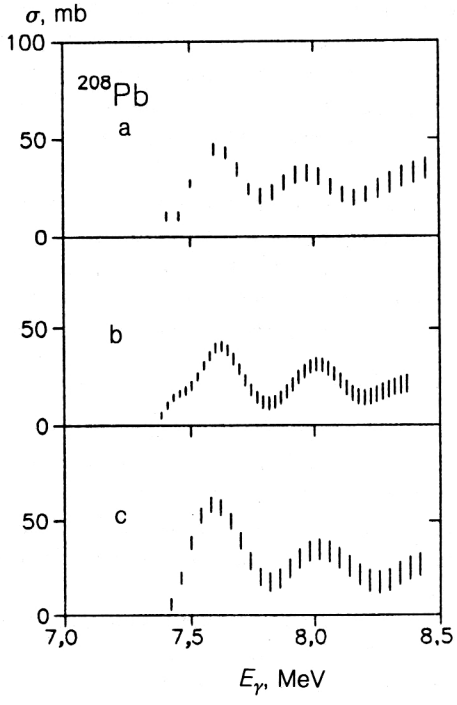

FIG. 2. Cross section of (γ,n) reaction on ^{208}Pb with measurement steps: a) 50 keV, b) 25 keV, c) 40 keV.

where samples with step 10, 20, 40, and 80 keV have been taken from the yield measured with step 10 keV and the cross section obtained from them. Clearly, one can say that there is a choice of the measurement step and level of the

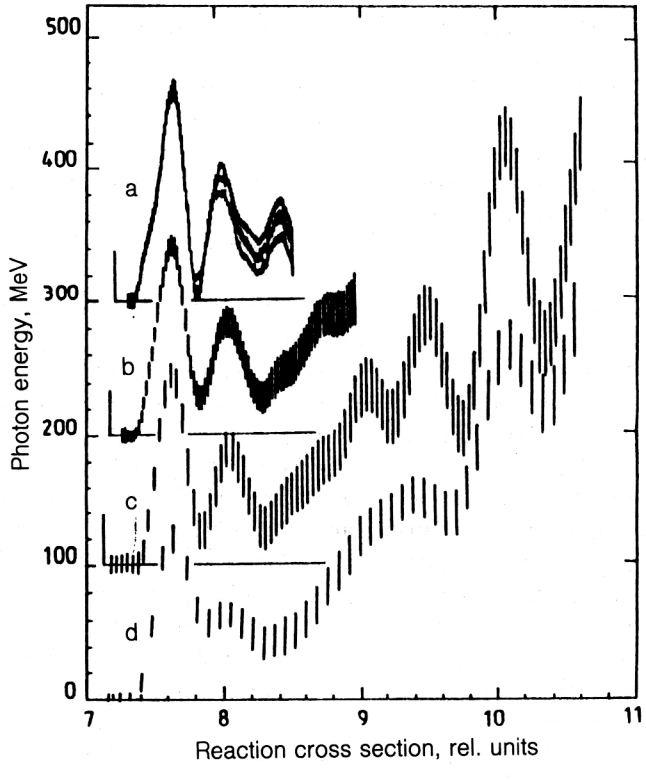

FIG. 3. Fragments of cross section of (γ,n) reaction on ^{208}Pb with measurement steps: a) 10 keV, b) 20 keV, c) 80 keV.

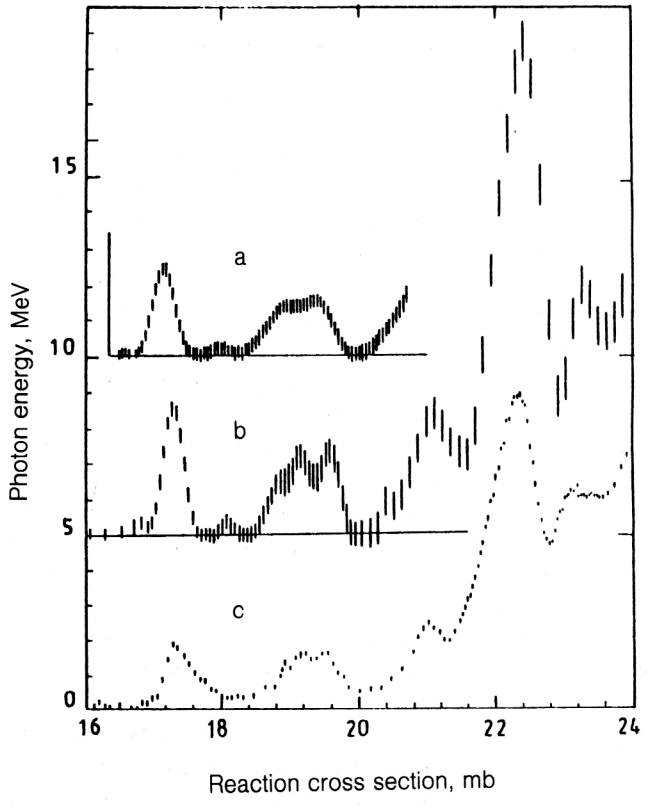

FIG. 4. Cross section of (γ,n) reaction on ^{16}O: a) data of Ref. 56, b) present study, c) data of Ref. 64.

statistics that are sufficient to resolve structures of a given magnitude (under the assumption that this magnitude can be characterized quantitatively). The problem is how to establish the correspondence.

If there exist suitable empirical data—experimental cross sections with approximately known resolution level—one can select the conditions of the measurements to obtain an analogous result. In Fig. 4, such a comparison is made with data on the cross section of the ^{16}O reaction[44] measured by the quasimonochromatic method with step 50 keV using a γ beam with resolution $\sim$200 keV at 24 MeV. Our measurements with step 50–60 keV have approximately the same resolution, but it can still be improved.

Another way to estimate the resolution is by a numerical experiment. This is done as follows. For a given model curve one generates for given conditions (energy step, statistical error) the yield curve, from which one recovers the model cross section, using the same computational procedure as in the real measurements. Varying the conditions or shape of the model curve, one can obtain the information needed to plan the experiment. Moreover, following in the process of the measurements the relationship between the changes in the yield and the level of the variance, one can, for a specific measurement step, correctly determine the time of completion of the experiment, obtaining at the same time the real resolution level for the given step. As the calculations show, if the rms error of the yield is $\approx$0.1–0.2 of the change of the yield $(Y_i - Y_{i-1})$ for step H_{meas} with respect to $E_{\gamma\,\max}$, peaks with widths at half-height of

order (2–4)H_{meas} in the model cross sections can be recovered, i.e., for measurements with step 40–60 keV it is entirely possible to resolve structures with widths of order 100 keV or more.

In model calculations, several narrow peaks of nearby energies are recovered as one broad resonance of asymmetric shape if the resolution is poor (large step or low accuracy). This effect is also possible under real conditions. Because the structure of the cross section can be formed by the superposition of several peaks, to find them (visually or by analysis) it is necessary that their amplitudes should not be small compared with the total value, and the shape of the line must be distorted sufficiently clearly.

There is a dependence of the resolution level on the position of the structures. From model estimates it can be seen that peaks in the initial sections of the model curve are, under otherwise identical conditions, recovered with better resolution than in the final sections. A possible reason for this is a decrease of the relative contribution from a structure to the yield with increasing energy of the structure. It may be that the structure leads to a change in the yield comparable with its error. The decrease in the amplitude of a peak in the recovered curve compared with the model curves may reach 10–15%, and peaks with width approximately equal to H_{meas} or less can disappear altogether. It should be noted that in the model calculations spurious structures did not appear, and it is important to know this when estimating the reliability of the experimental data.

6. ANALYSIS OF CROSS SECTIONS AND DETERMINATION OF PARAMETERS

To describe the structure of a cross section quantitatively, it is necessary to choose a mathematical model possessing parameters with a definite physical meaning that can be used to interpret the results and make a comparison with theoretical calculations. The assumption that the lines whose superposition may represent the cross section have a resonance nature is fairly well justified (both by theory and by experimental data). Each of the lines may, in its turn, be an envelope of resonances that are not resolved in the experiment. In this case, the quantities that will be compared with the theory and with analogous measurements will be the amplitude, width, and position of the given structure in the cross section, and also its contribution to the integrated cross section calculated from these parameters.

The choice of the type of resonance lines may be dictated by physical considerations or by actual features of the cross sections. An analogy with light nuclei is possible, since the assumed differences in the photoexcitation mechanism may have more to do with the number and structure of the excited states than with the actual form of the resonances.

A feature of the cross sections of (γ,n) reactions on medium and heavy nuclei is that resonance-type structures are superimposed on a rising base—the leading edge of a peak (or a sum of several peaks) of appreciably greater amplitude. Therefore, to obtain the parameters one employs a "residue separation" method, which consists of successive subtraction, from the total curve of the cross sections, of the lines calculated from their parameters, beginning with the line describing the main peak. In the approximation of the main peak, one uses points in the region of the maximum of the cross section and on its descending edge, since, as a rule, there are features in the cross section in the ascending branch right up to its maximum. At the same time, one approximates the cross section both by the traditionally employed Lorentz line and by the Gaussian one, which is better to analyze the curve of the reaction cross section on ^{208}Pb.

The physical significance of the procedure is in the selection and localization of the groups of excited states of the giant resonance at which the width of the states is much less than assumed ($\approx$3–4 MeV) at the given energies. The difference arises from the decrease of the contribution to the total width of the main term—the width of the transition to more complicated states. It should be noted that the experimentally determined widths may be overestimated if they are obtained for a grouping of levels with nearby energies that are not resolved under the conditions of the measurements. Difference in the structure of the excited states leads, in its turn, to the possibility of using lines of different types when decomposing the curve of the cross section into a superposition of resonance lines. The main strength of a state in which the simple configurations are weakly coupled to the more complicated ones will, because of the weak fragmentation, be concentrated in a narrow interval near its energy centroid. Such features in the shape of the cross section can be represented by Gaussian lines, whereas states with greater width form the base and can be separated by a line of Lorentz type.

7. THEORETICAL DESCRIPTION

Many reviews (Refs. 3–9 and 23–30) have been devoted to the problem of damping of giant multipole resonances. In analyzing the experimental data in this work we shall use the quasiparticle–phonon model, by means of which a fairly large range of nuclear excitations can be described from a common point of view. A detailed description of the model and a review of many theoretical studies can be found in Ref. 8. Here, we give only a brief schematic exposition of the model.

In the general case, the Hamiltonian of the model includes terms that describe the average field of the nucleus in the form of the Woods–Saxon potential, interactions that lead to pairing, and multipole–multipole and spin-multipole–spin-multipole isoscalar and isovector interactions, including charge-exchange interactions.

After a Bogolyubov canonical transformation, we introduce in the standard manner operators of phonons of multipolarity λ:

$$Q^{+}_{\lambda\mu i}=\tfrac{1}{2}\sum_{12}\{\psi^{\lambda i}_{12}A^{+}(12;\lambda\mu)-(-1)^{\lambda-\mu}\varphi^{\lambda i}_{12} \times A(12;\lambda-\mu)\}. \quad (4)$$

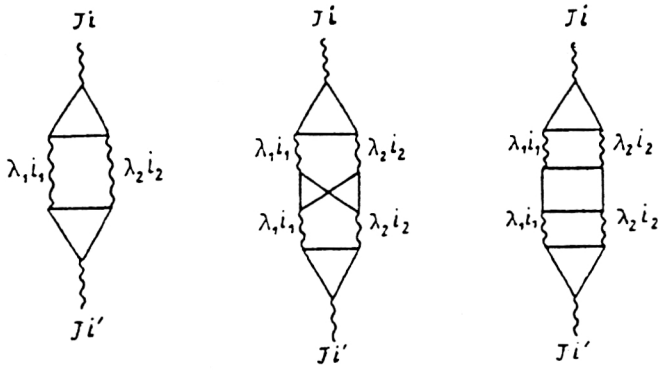

FIG. 5. Diagrams taken into account in the quasiparticle–phonon model in the description of the damping of giant multipole resonances.

Here, A^+ and A are bifermionic operators constructed from the quasiparticle creation and annihilation operators, respectively, and the phonon amplitudes ψ and φ are found by solving the corresponding equations of the random-phase approximation (RPA). The Hamiltonian of the quasiparticle–phonon model can be rewritten in terms of quasiparticle and phonon operators (see Ref. 8) and diagonalized on a basis of wave functions constructed in the form of an expansion with respect to the phonon operators. To describe the relaxation of the giant multipole resonance, one can make a restriction to a wave function in the form of a superposition of simple (single-phonon) and composite (two-phonon) configurations:

$$\Psi_\nu(JM)=\Big\{\sum_i R_i(J\nu)Q^+_{JMi}+\sum_{\lambda i\lambda' i'}P^{\lambda' i'}_{\lambda i}(J\nu) \times[Q^+_{\lambda\mu i}Q^+_{\lambda'\mu' i'}]_{JM}\Big\}\Psi_0. \quad (5)$$

Here, Ψ_0 is the ground-state wave function. The equations for determining the energies $\eta_{J\nu}$ of the state (4) and the coefficients R and P can be found, for example, in Ref. 4.

The diagrams shown in Fig. 5 are the most important ones for describing the damping of the resonance. The straight lines correspond to all possible hole and particle fermionic states, and the wavy lines to phonon states. The last diagrams arise when the Pauli principle is taken into account exactly, but their contribution is not that important for giant resonances.[45] All quantities needed to calculate the vertices and energy denominators can be expressed in terms of the parameters of the model Hamiltonian and the phonon amplitudes.[4]

With increasing excitation energy, there is a rapid increase in the density of levels, and a large fraction of the experimental information on highly excited states is represented in the form of quantities averaged or summed in definite energy intervals. Therefore, direct calculation of averaged quantities is more effective, both from the computational point of view and from the point of view of the analysis of the experimental data.

Let $\Phi_{J\nu}$ be the amplitude for excitation of the state $\Psi(JM)$ in some physical process. The corresponding strength function is determined by

$$b(\Phi,\eta)=\sum_\nu |\Phi_{J\nu}|^2\frac{1}{2\pi}\frac{\Delta}{(\eta-\eta_{J\nu})^2+\Delta^2/4}. \quad (6)$$

Here, Δ is the interval of the energy averaging. An exact expression for $b(\Phi,\nu)$ can be found in Ref. 8.

There is an intimate connection between strength functions and the functions of the response to an external field.[5,7] In the case of excitation of the state $\Psi_\nu(JM)$ by γ rays, the expression for $\Phi_{J\nu}$ has the form

$$\Phi_{J\nu}=\langle\Psi_0\|M[EJ(MJ)]Q^+_{J\mu i}\|\Psi_0\rangle, \quad (7)$$

where $M[EJ(MJ)]$ is the operator of the electric (magnetic) transition of multipolarity J (see Ref. 8).

The photoabsorption cross sections are related to the strength functions. For example, the dipole photoabsorption cross section averaged over the energy can be represented in the form

$$\sigma_{\gamma t}(E_\gamma)=4{,}025E_\gamma b(E1,E_\gamma), \quad (8)$$

where $\sigma_{\gamma t}$ is measured in millibarns, E_γ is the photon energy in mega-electron-volts, and the dipole strength function $b(\mathrm{E1},E_\gamma)$ is measured in the units $e^2\cdot\mathrm{fm}^2$.

All the calculations presented in this paper were made by means of a modified program GIRES.[46] We used the parameters of the Woods–Saxon potential and pairing constants from Refs. 23, 26, and 47. For example, for ^{208}Pb the single-particle spectrum was chosen in such a way as to reproduce in the framework of the quasiparticle–phonon model the energies, transition probabilities, and spectroscopic factors for the low-lying states of ^{208}Pb and the neighboring odd nuclei.[47] The constants of the dipole–dipole forces and multipole–multipole forces with Bohr–Mottelson radial dependence were chosen during the procedure mentioned above. The ratios of the isoscalar and isovector constants were fixed to reproduce the experimental values of the energies of the giant dipole resonances calculated in the RPA. The single-particle spectra include all quasibound levels with orbital angular momenta $l\leqslant 9$. The good description of the transition probabilities without the introduction of effective charges confirms the completeness of the employed basis. For example ,our calculations of the integrated properties of the giant dipole resonance in Refs. 4 and 48 agree very well with calculations that take into account the single-particle continuum exactly.[27,28]

8. DISCUSSION OF THE RESULTS

The appearance of intermediate structure in the photoneutron cross sections is most probable for nuclei with closed or nearly closed shells. Therefore, the experimental data for reactions on the nuclei ^{90}Zr ($N=50$), ^{116,124}Sn ($Z=50$) and on the series of isotopes with $N=82$ (^{138}Ba, ^{139}La, ^{140}Ce, ^{141}Pr, ^{142}Nd, ^{144}Sm) and $A\sim 200$ ($^{206\text{-}208}$Pb, ^{209}Bi) are of the greatest interest.

The measurements of the yields of photoneutrons in reactions on ^{90}Zr were made with step 60 keV in the inter-

TABLE I. Properties of isotopes and also the separation energies for one and two neutrons and the density parameter a used in the calculations.

Isotope	B_n, MeV	B_{2n}, MeV	a, MeV^{-1}	Mass, g	Thickness, g/cm^2	Enrichment, %
^{90}Zr	11,987	21,924		50		97,1
^{116}Sn	9,567	17,101	4,68	31,893		97,6
^{124}Sn	8,442	14,436	4,51	38,063		97,1
^{138}Ba	8,611	15,516	4,04		3,75	99,8
^{139}La	8,761	16,1	3,80		2,44	99,986
^{140}Ce	9,201	16,657	6,0		4,11	99,3
^{141}Pr	9,371	17,323	7,26		4,0	99,9
^{142}Nd	9,812	17,9	3,44		3,09	95,7
^{144}Sm	10,549	19,002	6,0	10		86
^{208}Pb	7,368	14,109	3,37		2,52	99
^{207}Pb	6,741				5,18	93,2
^{206}Pb	8,080				3,34	94,3
^{209}Bi	7,454				14,88	100

val of energies $E_{\gamma\,\max}$ from the reaction threshold to 21 MeV (see Table I, where we give the values of B_n and B_{2n}, taken from Ref. 49, for all the above nuclei together with properties of the targets and the values of the level-density parameter used for the correction for the multiplicity). The resulting cross section is shown in Fig. 6 and compared with data[50] measured using a quasimonochromatic beam. No manifestations of structure are observed on the leading edge of the cross section (if one does not count the threshold singularity). There is not agreement with the results of Ref. 50 in the region of the maximum. With regard to the descent from the resonance, the considered cross sections are correlated in the manifestation of substructures at energies near 17.5 and 19.5 MeV. It may be noted that our measurements in the bremsstrahlung beam do not give the structure in the cross section that was obtained in Ref. 51 in measurements by the same method. There is some agreement in the global behavior, but in our data there are no narrow (with widths of the order of hundreds of kilo-electron-volts) peaks.

Measurements of cross sections of the reactions on ^{116}Sn and ^{124}Sn were made under analogous conditions (60 keV for $E_{\gamma\,\max}$ and range up to 18 MeV). The measured cross sections are shown in Figs. 7 and 8 and compared with measurements made with a quasimonochromatic beam.[52,53] In the interval of energies from the threshold to the maximum, the shapes of the curves are complicated for all the cross sections. On the descent of the cross section of the reaction on ^{116}Sn there is a very weak feature at energy $\approx$17.5 MeV which correlates with the data of Refs. 52 and 53 at somewhat higher energies. However, this shift in

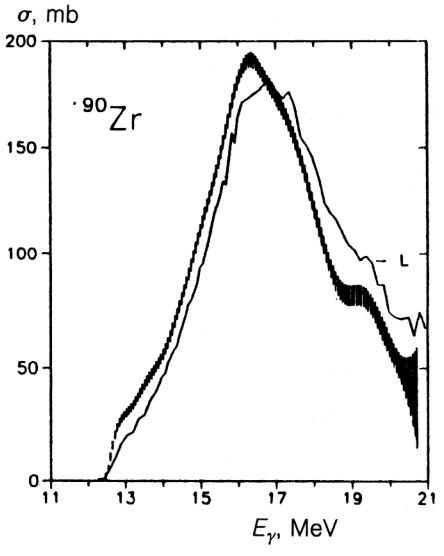

FIG. 6. Cross section of (γ,n) reaction on ^{90}Zr. The vertical strokes represent the present study; the continuous curve is from Ref. 50.

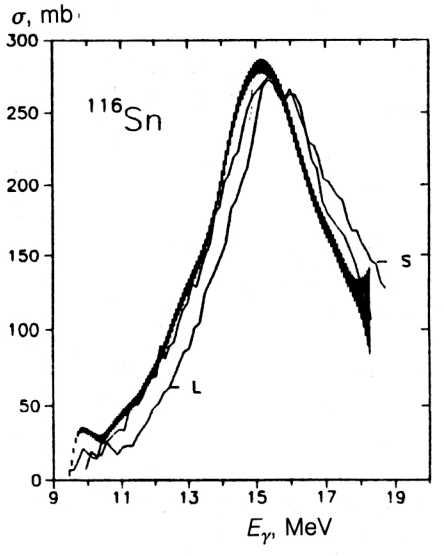

FIG. 7. Cross section of (γ,n) reaction on ^{116}Sn. The vertical strokes represent the present investigation, the continuous curve L is from Ref. 52, and the continuous curve S from Ref. 53.

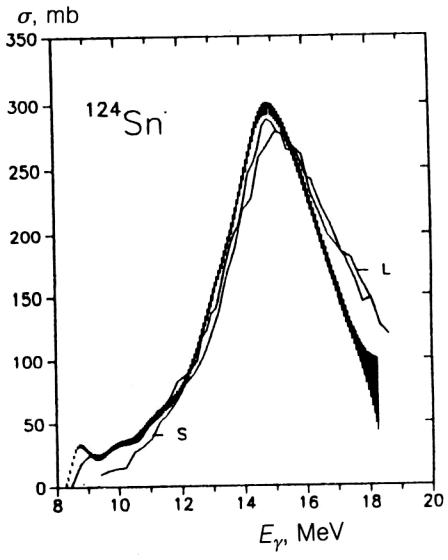

FIG. 8. Cross section of (γ,n) reaction on ^{124}Sn (legends as in Fig. 7).

energy is a consequence of the nonidentity of the energy scales for the cross section as a whole.

In our measurements, several features in the shape of the cross sections are observed in the ascending branch of the giant dipole resonance for both isotopes. Their amplitudes and widths can be estimated only in the case of decomposition of the cross section as a whole, but the approximate positions of the substructures can be readily determined visually, so that they can be compared subsequently with features calculated theoretically. The very fact of their existence on the ascending branch up to the region of the maximum shows that even for this region of the cross section it will be difficult to obtain a description

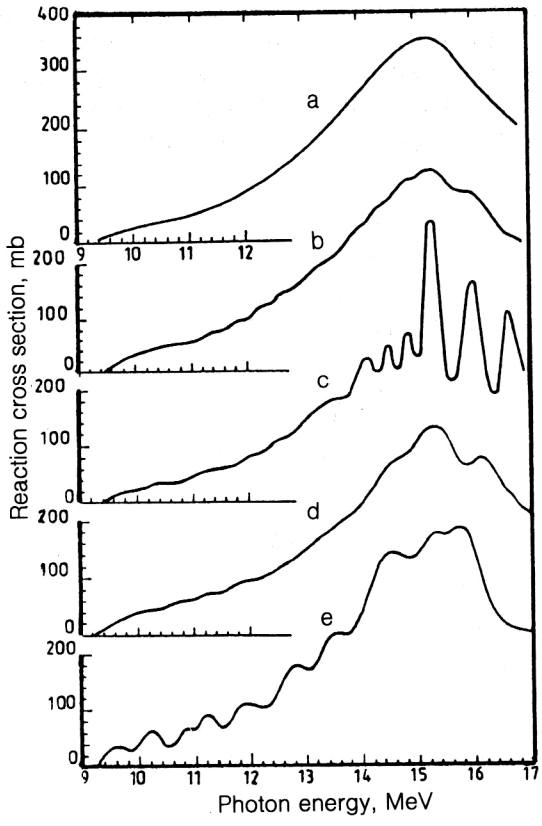

FIG. 9. Cross section of (γ,n) reaction on ^{141}Pr. Data from: a) Ref. 17, b) Ref. 18, c) Ref. 19, d) Ref. 20, e) Ref. 21.

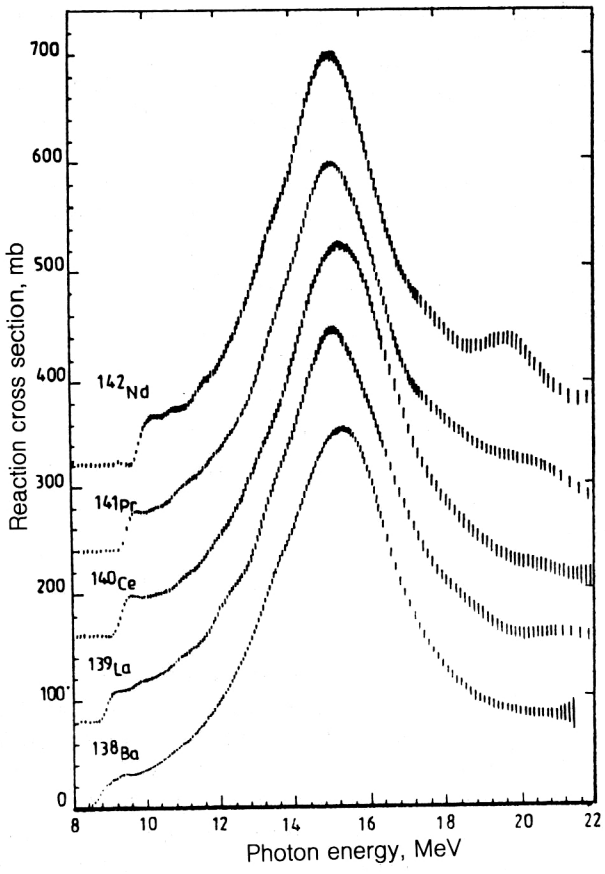

FIG. 10. Cross section of (γ,n) reaction on ^{138}Ba, ^{139}La, ^{140}Ce, ^{141}Pr, ^{142}Nd (data of Ref. 6).

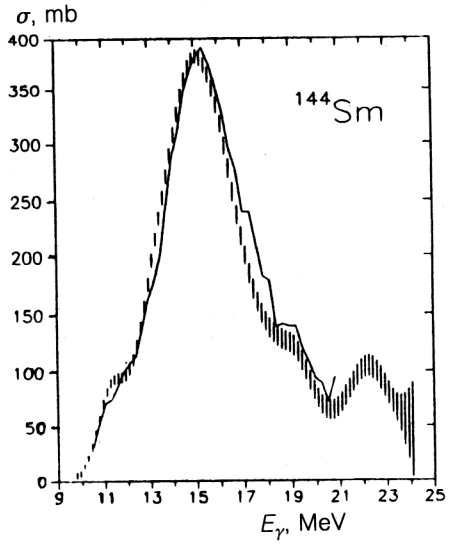

FIG. 11. Cross section of (γ,n) reaction on ^{144}Sm. The vertical strokes represent the present study, and the continuous curve is from Ref. 55.

by means of a Lorentz line, and the resulting parameters will inadequately characterize the cross section as a whole. In Ref. 53, a sum of two Lorentz lines (their widths were taken to be equal) was used for fitting, and this improved the description of the cross section in the energy range 13–18 MeV, but there was still a discrepancy between the cross sections and the line approximating them in the "tails" of the giant dipole resonance.

The cross sections of (γ,n) reactions on nuclei having closed neutron shells ($N=82$) have been studied quite intensively by both methods: quasimonochromatic and bremsstrahlung. Discrepancies are present in the results obtained by different groups, and they are especially appreciable for ^{141}Pr (see Fig. 9). Therefore, in the reactions on the ^{138}Ba, ^{139}La, ^{140}Ce, ^{141}Pr, ^{142}Nd nuclei,[54] and also on ^{144}Sm, we made measurements of the photoneutron yields by the bremsstrahlung method under conditions of the experiment that permitted study of intermediate structure in the form of the cross sections. The step of the measurements for all the nuclei (except ^{144}Sm) was 60 keV from the reaction threshold to energies $\approx$16–17 MeV, and then 120 keV. The measurements of the cross sections in the reactions on ^{144}Sm were made with the same step throughout the range, 160 keV, and therefore for ^{144}Sm the resolution in the measured cross section is not quite so good.

Figures 10 and 11 show the cross sections. In Fig. 11, the data for ^{144}Sm are compared with the results of Ref. 55 (continuous curve connecting the experimental points). It can be seen from Fig. 10 that the cross sections do not exhibit any appreciable and well-resolved substructures, but their form is not smooth. In the ascending branch of the dependences there are a number of features whose positions differ, though the number of them is approximately the same. The manifestation of the structural features, in both the ascending and descending branches in the curves of the cross section, is different for each of the nuclei de-

TABLE II. Parameters of Gaussian lines whose sum approximates the experimental cross section.

Nucleus	E, MeV	σ, mb	δ*, MeV	Contribution, %
^{138}Ba	9,1	18	0,3	0,8
	10,0	23	0,6	1,9
	11,9	62	1,0	9,4
	13,2	40	0,6	3,4
	15,3	355	1,4	70,3
	18,9	91	1,1	14,3
^{139}La	9,2	19	0,2	0,4
	9,7	25	0,4	1,2
	11,0	51	0,7	4,2
	12,3	68	0,6	4,7
	13,4	34	0,4	1,5
	15,1	363	1,4	59,1
	18,0	74	1,0	8,8
	21,3	83	2,0	19,7
^{140}Ce	9,6	24	0,2	0,6
	10,0	24	0,3	1,0
	10,8	29	0,5	2,0
	12,0	57	0,7	5,2
	13,3	32	0,5	2,1
	15,3	362	1,5	70,7
	18,4	52	0,9	5,9
	20,8	61	1,5	12,4
^{141}Pr	9,7	22	0,2	0,5
	10,1	22	0,3	0,8
	11,0	44	0,6	3,3
	12,3	69	0,7	6,2
	13,4	29	0,4	1,5
	15,1	355	1,3	62,4
	18,0	53	0,9	6,2
	20,1	79	1,8	19,1
^{142}Nd	10,1	31	0,2	0,8
	10,6	41	0,3	1,8
	11,6	61	0,5	4,0
	12,6	67	0,5	4,3
	13,4	38	0,3	1,7
	15,1	377	1,3	62,6
	17,6	70	0,7	7,0
	19,7	113	1,2	17,8
^{144}Sm	9,1	9	0,4	0,4
	11,3	70	0,6	4,8
	12,9	30	0,5	1,9
	15,1	381	1,6	67,4
	19,0	103	1,1	12,6
	22,3	103	1,1	12,8

TABLE III. Parameters of Gaussian lines whose sum, added to the Lorentz line, approximates the experimental cross section.

Nucleus	E, MeV	σ, mb	δ, MeV	Γ, GeV	Contribution, mb·MeV	Contribution, %
^{138}Ba	9,26 ± 0,02	9 ± 1	0,27 ± 0,01	0,64	6,1	0,28
	10,32 ± 0,06	9 ± 1	0,65 ± 0,03	1,53	14,3	0,65
	12,24 ± 0,03	29 ± 1	0,95 ± 0,02	2,23	68,9	3,15
	13,53 ± 0,02	35 ± 2	0,60 ± 0,02	1,40	52,4	2,39
	15,29 ± 0,01	357 ± 1	—	3,66	2047,7	95,53
^{139}La	9,22 ± 0,02	6 ± 1	0,32 ± 0,11	0,74	4,8	0,20
	9,92 ± 0,30	8 ± 1	0,92 ± 0,30	2,16	18,4	0,74
	11,00 ± 0,06	9 ± 1	0,92 ± 0,31	2,16	20,6	0,84
	12,24 ± 0,04	22 ± 1	1,16 ± 0,20	2,74	64,0	2,60
	13,37 ± 0,03	20 ± 2	0,75 ± 0,12	1,76	37,6	1,50
	15,12 ± 0,01	364 ± 1	—	3,70	2115,6	85,40
	16,90 ± 0,70	9 ± 3	0,70 ± 0,70	1,70	16,2	0,65
	18,50 ± 0,50	11 ± 7	0,60 ± 0,50	1,44	16,8	0,68
	21,90 ± 0,30	43 ± 3	1,70 ± 0,40	3,93	180,0	7,26
^{140}Ce	9,6 ± 0,2	12 ± 2	0,15 ± 0,01	0,36	4,4	0,20
	10,1 ± 1,0	9 ± 1	0,35 ± 0,04	0,82	7,4	0,33
	11,2 ± 0,2	8 ± 1	0,40 ± 0,05	0,94	8,0	0,36
	12,0 ± 0,1	6 ± 1	0,25 ± 0,04	0,58	3,6	0,16
	13,1 ± 0,1	26 ± 1	0,82 ± 0,02	1,93	53,4	2,39
	15,3 ± 0,1	364 ± 1	—	3,77	2153,3	95,65
^{141}Pr	9,75 ± 0,02	10 ± 2	0,11 ± 0,02	0,26	2,7	0,12
	10,10 ± 0,08	8 ± 1	0,25 ± 0,03	0,58	4,8	0,22
	11,03 ± 0,07	11 ± 1	0,42 ± 0,03	0,98	11,5	0,53
	12,29 ± 0,05	19 ± 1	0,67 ± 0,03	1,57	31,1	1,44
	13,32 ± 0,03	18 ± 1	0,35 ± 0,03	0,82	15,2	0,71
	15,09 ± 0,01	356 ± 1	—	3,56	1989,0	92,15
	18,50 ± 0,20	13 ± 5	0,50 ± 0,20	1,19	16,9	0,78
	20,40 ± 0,20	33 ± 2	1,10 ± 0,20	2,50	87,2	4,04
^{142}Nd	10,17 ± 0,03	15 ± 5	0,14 ± 0,03	0,33	5,2	0,23
	10,70 ± 0,10	16 ± 3	0,33 ± 0,13	0,77	13,0	0,58
	11,60 ± 0,10	12 ± 10	0,23 ± 0,12	0,54	6,7	0,30
	12,60 ± 0,80	24 ± 7	0,60 ± 1,00	1,48	37,3	1,66
	13,40 ± 0,10	20 ± 50	0,30 ± 0,30	0,75	16,5	0,73
	15,04 ± 0,01	356 ± 1	—	3,39	2011,0	89,50
	17,88 ± 0,13	15 ± 4	0,40 ± 0,10	0,94	14,8	0,66
	19,86 ± 0,60	61 ± 3	0,90 ± 0,10	2,17	141,5	6,30
^{144}Sm	11,31 ± 0,04	28 ± 3	0,38 ± 0,05	0,90	79,3	2,94
	13,34 ± 0,08	25 ± 3	0,54 ± 0,08	1,26	33,3	1,24
	15,12 ± 0,03	385 ± 3	—	3,95	2388,4	88,62
	19,14 ± 0,09	33 ± 4	0,55 ± 0,09	1,27	44,4	1,65
	22,38 ± 0,07	67 ± 4	0,88 ± 0,08	2,08	149,3	5,54

spite such slight differences in A. Moreover, the positions of the maxima in the curves for ^{138}Ba and ^{140}Ce are shifted relative to the remainder by about 200 keV to higher energies.

In Ref. 54, quantitative estimates for the substructures were obtained by approximating the cross sections by a sum of Gaussian lines:

$$\sigma(\gamma,n)=\sum_i \sigma_0^i \exp[-(E-E_0^i)^2/2\delta_i^2], \qquad (9)$$

where σ_0^i, E_0^i, δ_i characterize the amplitude, position, and width of the resonances forming the cross section; δ_i is the square root of the variance of the corresponding distribution and is related to the width at half-height, Γ_i, by $\Gamma_i=2.335\delta_i$.

Table II gives these parameters together with the data of the approximation of the high-energy tails of the cross sections and the analogous parameters for ^{144}Sm. The amplitude and width parameters of the resonances enabled us to estimate the relative contribution of each of them to the integrated cross section of the giant dipole resonance, which was determined by adding the areas under the Gaussian lines. The cross sections were also described similarly (on the basis of the ideas in Sec. 6) by using a Lorentz line to approximate the region of the cross-section maximum. Table III gives the parameters of the lines together with the absolute and relative contributions to the integrated cross section; the area under a Lorentz line was taken to be its analytic value $\pi/2\sigma\Gamma$ calculated from the parameters.

We shall consider the photoneutron cross sections of the reactions on $^{206-208}$Pb and ^{209}Bi, paying particular attention to ^{208}Pb, since for this nucleus there are many experimental data and theoretical calculations. The shape of

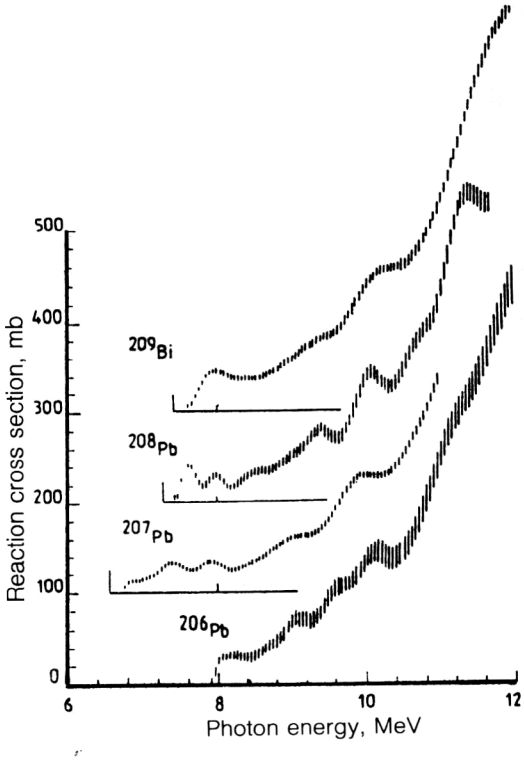

FIG. 12. Cross section of (γ,n) reactions on ^{206,207,208}Pb and ^{209}Bi at energies up to 12 MeV (data of Ref. 56).

the (γ,n)-reaction cross section in the ascending branch of the giant dipole resonance for the lead and bismuth in the range of excitation energies from the reaction threshold to ≈ 12 MeV was studied in a bremsstrahlung experiment.[56] The properties of the targets are given in Table I. The measurement step was about 50 keV, and the relative error in the photoneutron yield at the upper energy level was near 0.3%. The measured cross sections are shown in Fig. 12. It can be seen that all the curves have structures in the form of peaks that are resolved to a greater or lesser degree and are superimposed on the rising base. Under the assumption of a resonance nature of the cross section as a whole, the shape of the base was modeled by a sum of two lines: an exponential (for ^{208}Pb) or a parabola (for the remaining nuclei) with values decreasing to zero near the reaction threshold and a Lorentz line calculated from the parameters: $\sigma=640$ mb, $E=13.42$ MeV, $\Gamma=3.6$ MeV. In this way it is possible to obtain quantitative estimates of the structures in the cross sections by subtracting the base and approximating the remaining parts by a set of Gaussian lines.

The parameters of the Gaussian lines and the contributions, calculated on their basis, of the resonances of the intermediate structure are given in Table IV. Because of the unavoidable arbitrariness in the separation of the base, it is obvious that in such a procedure there can be systematic errors in the values of the parameters. However, this mainly applies to the values of the amplitudes and widths; the positions of the resonances remain practically unchanged. It should be noted that the level of the experimental resolution has a similar influence on the parameters of the structures. Table V gives estimates of the positions and widths of the structures in the cross section of the reaction on ^{208}Pb obtained in (γ,n) (Refs. 56, 15, and 16), (e,e') (Refs. 57 and 58), and (γ,γ') (Ref. 59) reactions. It can be seen that there are large discrepancies in the widths, whereas the positions of the resonances agree well. Therefore, one may hope that for ^{206,207}Pb and ^{209}Bi the energy positions of the structures are at least correct estimates.

In Ref. 54, the cross section of the (γ,n) reaction on ^{208}Pb, measured under the same conditions with which the data in Ref. 56 were obtained and with the same target, was considered. The only differences were in the range of the measurements (it was increased to 22 MeV) and the measurement step. The step with respect to the limiting energies $E_{\gamma\,\max}$ for the interval from the neutron emission threshold to 8.5 MeV was 40 keV, up to 12 MeV it was 60 keV, and then 120 keV. The order of the scanning with respect to the energy was specified to compensate the low neutron yield in the threshold region of energies by a large number of measurements in these channels. In Fig. 13, the cross section from Ref. 56 is compared with the data from Ref. 54. It can be seen that the structures in the ascending branch of the cross section are well reproduced, although they differ somewhat in form. This can be explained by a certain difference in the resolution level resulting from the differences in the measurement step and statistics. For measurement step 25 keV (Fig. 13a), one can see in the cross section at energy ≈ 7.43 MeV a poorly resolved peak, which can also be seen in Fig. 3a as a feature in the leading edge of the resonance with energy 7.6 MeV.

Qualitative comparison with the results of other measurements of the (γ,n)-reaction cross section on ^{208}Pb reveals both an agreement and appreciable discrepancies in the shape of the structures in the curves in the leading edge. In Fig. 14, the data of Ref. 56 are compared with cross sections obtained in measurements using a quasimonochromatic γ-ray beam.[14,15] The agreement of the results of Refs. 56 and 15 is completely obvious, both for the number and position and also for the shape of the structures, whereas in Ref. 14 only the peak at energy ≈ 11 MeV is clearly manifested. The bremsstrahlung measurements of Ref. 16 also agree well in the interval 9–12 MeV with the data of Ref. 54 (see Fig. 15) in the shape, but the structures are shifted upward in energy by about 200 keV. We also show here (Fig. 15c) the data of Ref. 60 obtained by the tagged-photon method, which show the presence of structure at energies ≈ 10 and 10.6 MeV.

In Table VI we give the parameters obtained from the description of the cross sections of (γ,n) reactions on ^{208}Pb by a set of Gaussian lines.[54]

On the basis of these parameters, we determined the relative contributions of the peaks to the integrated cross section (as percentages), which was calculated as the sum of the areas under the Gaussian lines. The absolute values (in mb · MeV) of the contributions of the individual peaks are given by the areas under the corresponding Gaussian lines. This method of decomposition is dictated by the shape and number of the observed structures. The use of Lorentz or Breit–Wigner lines gives an unsatisfactory re-

TABLE IV. Parameters of Gaussian lines of the estimate of the contributions to the integrated cross section of the intermediate-structure resonances.

Nucleus	E, MeV	σ, mb	δ*, MeV	σ_{int}, mb · MeV
^{206}Pb	8,1	21	0,17	8,79
	8,6	9	0,10	2,17
	9,0	22	0,14	7,88
	9,5	25	0,14	8,96
	10,0	34	0,17	14,44
	11,0	70	0,28	49,13
	11,8	95	0,38	90,49
				$\sum \sigma_{int} = 181,86$
^{207}Pb	6,9	13	0,08	2,74
	7,1	8	0,10	1,93
	7,4	29	0,18	12,72
	7,9	21	0,15	8,00
	8,9	10	0,18	4,39
	9,8	30	0,19	14,51
	11,6	110	0,50	137,90
				$\sum \sigma_{int} = 182,19$
^{208}Pb	7,6	38	0,10	9,05
	8,0	20	0,10	4,76
	8,5	10	0,16	4,14
	9,0	12	0,13	3,91
	9,3	26	0,13	8,47
	10,0	46	0,15	17,64
	10,6	22	0,15	8,16
	11,3	93	0,22	52,20
				$\sum \sigma_{int} = 108,35$
^{209}Bi	7,9	35	0,16	13,69
	8,2	14	0,13	4,63
	8,5	8	0,13	2,65
	8,8	6	0,14	2,17
	9,3	13	0,19	6,29
	10,1	35	0,28	24,24
	11,3	95	0,41	97,16
				$\sum \sigma_{int} = 150,77$

*Width at half-height $\Gamma = 2.355\delta$.

sult. Under the assumption that the main peak, the maximum of which coincides with the maximum of the cross section, is formed by one such line it is not possible to separate completely the structures in the leading edge on account of the large width of this peak.

We consider above all the theoretical description of the integrated characteristics of the giant dipole resonance in ^{208}Pb. For the energy interval 10.0–17.0 MeV, we obtained for the energy centroid $E_x = 13.35$ MeV, for the width $\Gamma = 3.5$ MeV, and 80% exhaustion of the model-independent energy-weighted sum rule (the calculations were made for $\Delta = 1$ MeV); for the experimental values of Ref. 1, these quantities are $E_x = 13.46$ MeV, $\Gamma = 3.9$ MeV, and 89%, respectively). As can be seen from Fig. 16, a good overall description of the experimental cross section is obtained. A certain overestimation of the cross section at the maximum and underestimation of the high-energy part can be attributed to the fact that in the actual calculation many two-phonon states weakly coupled to the single-phonon states must be ignored because of the high density

TABLE V. Properties of resonances in ^{208}Pb obtained in different reactions.

Reaction	Energy and width of resonance (given in brackets), MeV								Reference
(γ, n)	7,60 (0,23)	8,00 (0,23)	8,50 (0,38)	9,00 (0,31)	9,30 (0,31)	10,0 (0,35)	10,6 (0,35)	11,3 (0,52)	[56]
(γ, n)	7,60	8,00	8,30			9,90		11,2	[15]
(γ, n)			8,85	9,15	9,60	10,25	10,8	11,45	[16]
(e, e')	7,3	7,9		8,9		10,2	10,6	11,2	[57]
(e, e')				8,9	9,4	10,0 (0,47)	10,6 (0,71)	11,2 (0,88)	[58]
(γ, γ')						10,0 (0,16)	10,6 (0,23)	11,3 (0,33)	[59]

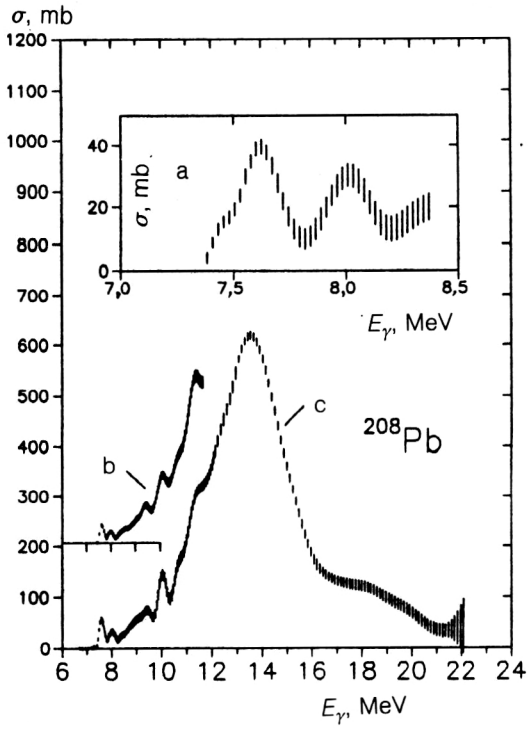

FIG. 13. Cross section of (γ,n) reaction on ^{208}Pb. Measurement step: a) 25 keV, b) 50 keV (Ref. 54), c) 40 keV from the photoneutron threshold to 9 MeV, 60 keV to 12 MeV, and then 120 keV.

and computational limitations. To a significant extent, their integrated contribution can be taken into account by increasing the energy averaging parameter Δ. The same figure shows the results of calculating the distribution of the dipole strength in the random-phase approximation. As

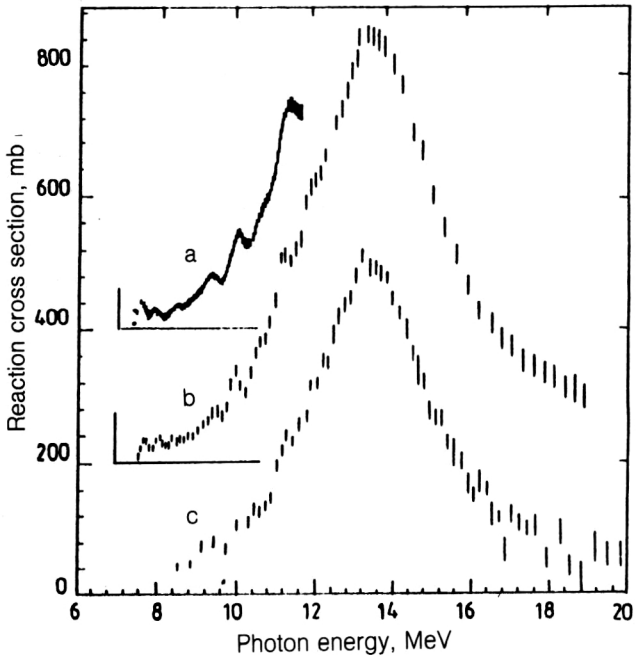

FIG. 14. Cross sections of (γ,n) reaction on ^{208}Pb obtained in: a) Ref. 56, b) Ref. 15, c) Ref. 14.

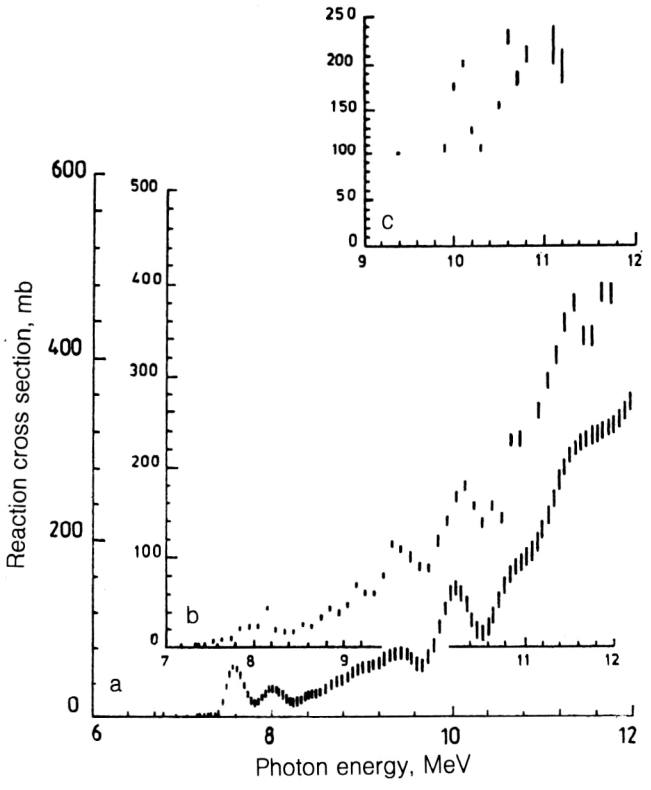

FIG. 15. Cross sections of (γ,n) reaction on ^{208}Pb obtained in: a) Ref. 56, b) Ref. 16, c) Ref. 60.

can be seen from Figs. 13 and 16, in the low-energy part of the cross section there are substructures with positions very close to the collective states of the RPA. The coupling to the two-phonon states leads to a redistribution of the dipole strength; moreover, in the low-energy region, where the density of states is relatively low, the substructures are more clearly defined. In the high-energy region, there is complete smoothing of the cross sections.

As we already mentioned, the substructures are most clearly manifested in the low-energy part of the tail of the giant dipole resonance (see Fig. 17). To clarify the position with regard to the substructures, we made calculations with a smaller energy averaging parameter for this region. Figure 17 presents the results of our calculations of the cross sections obtained with smearing parameter $\Delta=0.2$ MeV, corresponding approximately to the experimental conditions. The theoretical calculations reproduce the main substructures at the excitation energies 7.6, 8.6, 9.1, 9.5, 10, and 11.3 MeV (see Table III). In the case of the substructure at 7.6 MeV, not only the E1 transitions (broken curve) but also the isovector M1 resonance, which was investigated in the framework of the quasiparticle–phonon model in Ref. 61, makes an important contribution. This agrees well with experimental data obtained with polarized tagged photons.[62] The substructure at 8 MeV is not reproduced in our calculations, although, as can be seen from Fig. 17, there is a two-hump structure of the E1 cross section at lower energy. Our old calculations in Ref. 63 also indicate the presence of two peaks in the interval 7–8

TABLE VI. Parameters of representation of photoneutron cross section by a set of Gaussian lines and contributions of individual resonances to the integrated cross section.

N	σ, mb	E, MeV	δ, MeV	Γ^*, MeV	Contribution, mb · MeV	Contribution, %
1	61±2	7,60±0,01	0,095±0,003	0,22	14,3	0,49
2	31±3	8,00±0,02	0,135±0,014	0,32	10,5	0,36
3	31±4	8,64±0,06	0,304±0,026	0,72	23,7	0,81
4	50±4	9,14±0,05	0,235±0,015	0,55	29,3	1,00
5	51±6	9,47±0,03	0,141±0,015	0,33	17,9	0,61
6	133±3	10,03±0,02	0,215±0,018	0,51	71,7	2,45
7	76±22	10,63±0,03	0,176±0,041	0,41	33,7	1,15
8	179±4	11,33±0,03	0,422±0,076	0,99	189,4	6,47
9	48±15	12,20±0,10	0,260±0,076	0,61	31,0	1,06
10	618±4	13,56±0,02	1,227±0,063	2,89	1902,6	65,00
11	54±4	16,00±0,10	0,834±0,040	1,96	114,0	3,86
12	117±3	18,20±0,08	1,688±0,044	3,98	494,7	16,90

*Width at half height $\Gamma = 2.355\delta$.

MeV. These differences can be attributed to inaccuracies in the single-particle energies, but it was not our aim to achieve a perfect description of the experimental data, and we used the single-particle spectrum from our earlier study. The E2 transitions make a contribution to the photoneutron cross section that can hardly be distinguished on the background of the E1 transitions.

The problem of the existence of substructures in nuclei in the region of lead was discussed in Ref. 63. Data obtained in γ-ray scattering experiments[59] indicate the presence of substructures in the photoabsorption cross sections in ^{206,208}Pb at energies below the neutron separation threshold. The calculations made using the quasiparticle–phonon model in Refs. 4 and 63 reproduce these substructures in these nuclei to a large degree correctly. In ^{206}Pb, compared with ^{208}Pb, the structures are significantly smoothed for energies above the neutron threshold. These theoretical predictions agree with the experimental data (see Ref. 63 and Fig. 12).

Figure 18 shows the experimental and theoretical photoabsorption cross sections for ^{90}Zr, ^{116}Sn, and ^{142}Nd. It can be seen that the calculations with large Δ reproduce the experimental data rather well. As we already noted, this is due to the fact that for such Δ one takes into account effectively the contribution of a large number of two-phonon states weakly coupled to the single-phonon states; in a realistic calculation, these cannot be included because of the computing limitations.

Our calculations with smaller Δ in the low-energy part of the ^{116,124}Sn and ^{142}Nd cross sections are shown in Fig. 19. In these nuclei, in contrast to lead, the substructures

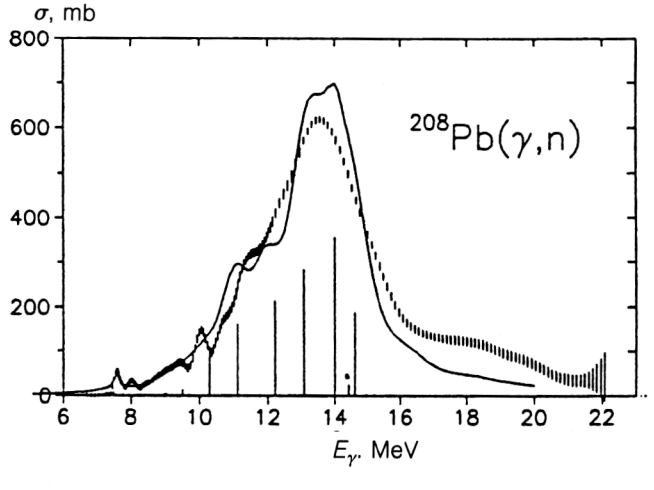

FIG. 16. Experimental (points) and theoretical (continuous curve, $\Delta = 1$ MeV) photoneutron cross sections in ^{208}Pb. The vertical strokes show the results of calculations in the random-phase approximation (in arbitrary units).

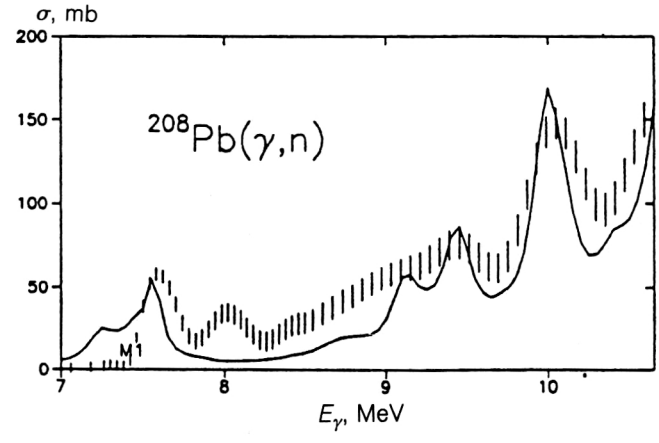

FIG. 17. Low-energy part of cross section (the points represent the experiment, and the continuous curve is a calculation with $\Delta = 0.2$ MeV of the sum of the cross sections of E1 and M1 photoabsorption).

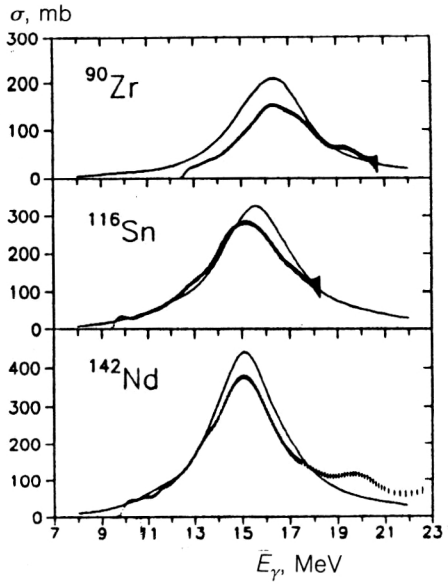

FIG. 18. Experimental (points) and theoretical (continuous curve, $\Delta=2$ MeV) photoneutron cross sections in ^{90}Zr, ^{116}Sn, ^{142}Nd.

practically disappear, although some traces of them are observed. As we noted earlier, because the vibrations in these nuclei are more strongly anharmonic there is a redistribution of the electromagnetic strengths between the individual RPA states, and the substructures are smoothed. These conclusions are clearly confirmed by the complete set of existing experimental data.

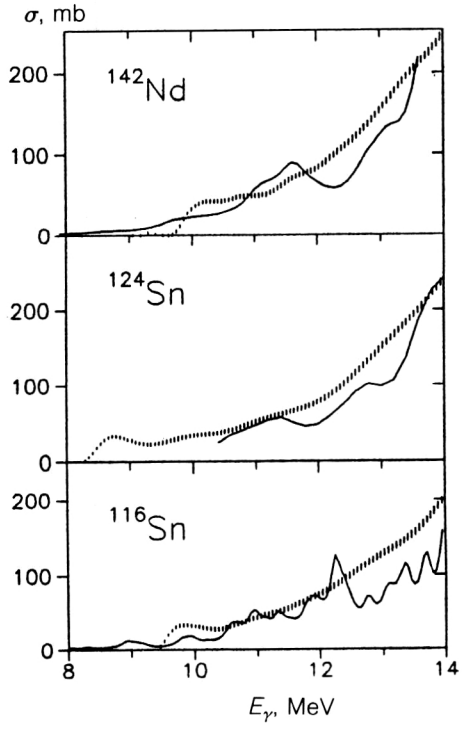

FIG. 19. Experimental (points) and theoretical [continuous curve, $\Delta=0.5$ MeV (0,2 for ^{116}Sn)] photoneutron cross sections in ^{116}Sn, ^{124}Sn, ^{142}Nd.

9. CONCLUSIONS

On the basis of the investigations, we conclude that there is reliable identification of the substructures in the photoabsorption cross sections for nearly magic nuclei in the low-energy region. These substructures find a natural explanation from the microscopic point of view as being the result of nonuniform distribution of the electromagnetic strength. This nonuniform distribution is a consequence of individual features of the single-particle spectra of the nuclei and the coupling of the single-particle and collective degrees of freedom.

The experimental data indicate the presence of some structures in the photoabsorption cross sections at excitation energies around 20 MeV. It is possible that these substructures are associated with excitation of a giant dipole resonance with isospin $T_>$. However, this question requires an additional experimental and theoretical study, and that goes beyond the scope of this paper.

[1] B. L. Berman and S. C. Fultz, Rev. Mod. Phys. **47**, 713 (1975).
[2] F. E. Bertrand, Nucl. Phys. **A354**, 129 (1981).
[3] K. Goeke and J. Speth, Ann. Rev. Nucl. Part. Sci. **32**, 65 (1982).
[4] V. V. Voronov and V. G. Solov'ev, Fiz. Elem. Chastits At. Yadra **14**, 1380 (1983) [Sov. J. Part. Nucl. **14**, 583 (1983)].
[5] G. F. Bertch, P. F. Bortignon, and R. A. Broglia, Rev. Mod. Phys. **55**, 287 (1983).
[6] A. Van der Woude, Prog. Part. Nucl. Phys. **18**, 217 (1987).
[7] J. Wambach, Rep. Prog. Phys. **51**, 989 (1988).
[8] V. G. Solov'ev, *Nuclear Theory. Quasiparticles and Phonons* [in Russian] (Énergoatomizdat, Moscow, 1989).
[9] M. G. Urin, *Relaxation of Nuclear Excitations* [in Russian] (Énergoatomizdat, Moscow, 1990).
[10] R. Bergere, Lect. Notes Phys. **61**, 1 (1977).
[11] S. S. Dietrich and B. L. Berman, At. Data Nucl. Data Tables **38**, 199 (1988).
[12] A. Bohr and B. R. Mottelson, *Nuclear Structure*, Vols. 1 and 2 (Benjamin, New York, 1969, 1975) [Russ. transl., Mir, Moscow, 1971, 1977].
[13] E. G. Fuller and E. Hayward, Nucl. Phys. **23**, 431 (1962).
[14] R. R. Harvey *et al.*, Phys. Rev. **136**, B126 (1964).
[15] E. Veyssiere *et al.*, Nucl. Phys. **A159**, 561 (1970).
[16] R. Van der Vyver *et al.*, Z. Phys. A **284**, 91 (1978).
[17] R. E. Sund *et al.*, Phys. Rev. C **2**, 1129 (1970).
[18] H. Beil *et al.*, Nucl. Phys. **A172**, 426 (1971).
[19] P. H. Cannington *et al.*, Nucl. Phys. **A109**, 385 (1968).
[20] T. K. Deague *et al.*, Nucl. Phys. **A191**, 305 (1972).
[21] B. C. Cook *et al.*, Nucl. Phys. **A143**, 730 (1966).
[22] B. S. Ishkhanov *et al.*, Usp. Fiz. Nauk **160**, 57 (1990) [Sov. Phys. Usp. **33**, 204 (1990)].
[23] V. G. Soloviev *et al.*, Nucl. Phys. **A304**, 503 (1978).
[24] S. Adachi and Nguyen Van Giai, Phys. Lett. **149B**, 447 (1984).
[25] S. P. Kamerdzhiev *et al.*, Phys. Lett. **267B**, 12 (1991).
[26] V. G. Soloviev, *et al.*, Nucl. Phys. **A288**, 376 (1977).
[27] R. De Haro *et al.*, Nucl. Phys. **A388**, 265 (1982).
[28] V. V. Pal'chik *et al.*, Yad. Fiz. **34**, 903 (1981); **35**, 1374 (1982) [Sov. J. Nucl. Phys. **34**, 504 (1981); **35**, 801 (1982)].
[29] V. G. Solov'ev, Fiz. Elem. Chastits At. Yadra **9**, 860 (1978) [Sov. J. Part. Nucl. **9**, 343 (1978)].
[30] A. I. Vdovin and V. G. Solov'ev, Fiz. Elem. Chastits At. Yadra **14**, 237 (1983) [Sov. J. Part. Nucl. **14**, 99 (1983)].
[31] O. V. Bogdankevich, At. Energ. **12**, 198 (1962).
[32] S. N. Belyaev *et al.*, *Abstracts of Papers at the 25th Symposium on Nuclear Spectroscopy and Nuclear Structure* [in Russian] (Nauka, Leningrad, 1975), p. 423; *Abstracts of Papers at the 30th Symposium on Nuclear Spectroscopy and Nuclear Structure* [in Russian] (Nauka, Leningrad, 1980), p. 414; Prib. Tekh. Eksp. **1**, 18 (1980); **1**, 21 (1981); *Problems of Theoretical and Nuclear Physics* [in Russian] (Saratov State University, Saratov, 1982).
[33] V. F. Turchin *et al.*, Usp. Fiz. Nauk **102**, 345 (1970) [Sov. Phys. Usp. **13**, 681 (1971)].

[34] V. F. Turchin, Zh. Vychisl. Mat. Mat. Fiz. **7**, 1270 (1967).
[35] V. F. Turchin, Zh. Vychisl. Mat. Mat. Fiz. **8**, 230 (1968).
[36] V. F. Turchin and V. É. Novik, Izv. Akad. Nauk SSSR, Ser. Fiz. Atm. Okeana **5**, 29 (1969).
[37] V. F. Turchin and V. É. Novik, Preprint No. 138 [in Russian], Physics and Power Institute, Obninsk (1969).
[38] V. F. Turchin and L. S. Turovtseva, Dokl. Akad. Nauk SSSR **212**, 561 (1973).
[39] L. S. Turovtseva and V. F. Turchin, Preprint No. 30 [in Russian], Institute of Applied Mathematics, Moscow (1971).
[40] L. S. Turovtseva, Preprint No. 48 [in Russian], Institute of Applied Mathematics, Moscow (1975).
[41] S. N. Belyaev *et al.*, *Abstracts of Papers of the 32nd Symposium on Nuclear Spectroscopy and Nuclear Structure* [in Russian] (Nauka, Leningrad, 1982), p. 370.
[42] O. V. Bogdankevich and F. A. Nikolaev, *Working with Bremsstrahlung Beams* [in Russian] (Atomizdat, Moscow, 1964).
[43] J. M. Blatt and V. F. Weisskopf, *Theoretical Nuclear Physics* (Wiley, New York, 1952) [Russ. transl., IL, Moscow, 1954].
[44] J. T. Caldwell *et al.*, Phys. Rev. Lett. 976 (1965).
[45] V. V. Voronov *et al.*, Yad. Fiz. **40**, 683 (1984) [Sov. J. Nucl. Phys. **40**, 438 (1984)].
[46] V. Yu. Ponomarev *et al.*, Preprint R4-81-704 [in Russian], JINR, Dubna (1981).
[47] V. V. Voronov and Dao Tien Khoa, Izv. Akad. Nauk SSSR, Ser. Fiz. **48**, 2008 (1984).
[48] V. V. Voronov and V. Yu. Ponomarev, Nucl. Phys. **A250**, 619 (1990).
[49] V. L. Kravtsov, *Masses of Atoms and Nuclear Binding Energies* [in Russian] (Atomizdat, Moscow, 1974).
[50] B. L. Berman *et al.*, Phys. Rev. **162**, 1098 (1967).
[51] B. S. Ishkhanov and V. G. Shevchenko, Fiz. Elem. Chastits At. Yadra **3**, 894 (1972) [Sov. J. Part. Nucl. **3**, 446 (1972)].
[52] S. C. Fultz *et al.*, Phys. Rev. **186**, 1255 (1969).
[53] A. Lepretre *et al.*, Nucl. Phys. **A219**, 39 (1974).
[54] S. N. Belyaev and V. A. Semenov, Izv. Akad. Nauk SSSR, Ser. Fiz. **55**, 953 (1991).
[55] P. Carlos *et al.*, Nucl. Phys. **A225**, 171 (1974).
[56] S. N. Belyaev *et al.*, Yad. Fiz. **42**, 1050 (1985) [Sov. J. Nucl. Phys. **42**, 662 (1985)].
[57] F. R. Buskirk *et al.*, Phys. Lett. **42B**, 194 (1972).
[58] M. Nagao and J. Torizuka, Phys. Rev. Lett. **30**, 1068 (1973).
[59] R. D. Starr *et al.*, Phys. Rev. C **25**, 780 (1982).
[60] Z. W. Bell *et al.*, Phys. Rev. C **25**, 791 (1982).
[61] Dao Tien Khoa *et al.*, Preprint E4-86-198, JINR, Dubna (1986).
[62] R. M. Laszewski *et al.*, Phys. Rev. Lett. **61**, 1710 (1988).
[63] V. G. Soloviev *et al.*, Nucl. Phys. **A399**, 141 (1983).
[64] R. L. Bramblett *et al.*, Phys. Rev. **133**, 869 (1964).

Translated by Julian B. Barbour